Journal of Colloid and Interface Science **241,** 233–247 (2001)
doi:10.1006/jcis.2001.7743, available online at http://www.idealibrary.com on IDEAL®

The Dynamics of Marangoni-Driven Local Film Drainage between Two Drops

Leslie Y. Yeo, Omar K. Matar,[1] E. Susana Perez de Ortiz, and Geoffrey F. Hewitt

Department of Chemical Engineering and Chemical Technology, Imperial College of Science, Technology and Medicine, Prince Consort Road, London, SW7 2BY, United Kingdom

Received March 1, 2001; accepted May 31, 2001

A study of Marangoni-driven local continuous film drainage between two drops induced by an initially nonuniform interfacial distribution of insoluble surfactant is reported. Using the lubrication approximation, a coupled system of fourth-order nonlinear partial differential equations was derived to describe the spatio-temporal evolution of the continuous film thickness and surfactant interfacial concentration. Numerical solutions of these governing equations were obtained using the Numerical Method of Lines with appropriate initial and boundary conditions. A full parametric study was undertaken to explore the effect of the viscosity ratio, background surfactant concentration, the surface Péclet number, and van der Waals interaction forces on the dynamics of the draining film for the case where surfactant is present in trace amounts. Marangoni stresses were found to cause large deformations in the liquid film: Thickening of the film at the surfactant leading edge was accompanied by rapid and severe thinning far upstream. Under certain conditions, this severe thinning leads directly to film rupture due to the influence of van der Waals forces. Time scales for rupture, promoted by Marangoni-driven local film drainage were compared with those associated with the dimpling effect, which accompanies the approach of two drops, and implications of the results of this study on drop coalescence are discussed.

Key Words: **drop coalescence; insoluble surfactant; film drainage; film rupture; Marangoni effect; thin film; emulsions; stability.**

1. INTRODUCTION

In order for two drops approaching each other in a liquid–liquid dispersion to coalesce, the intervening continuous phase film trapped between the drops must drain to some critical thickness beyond which film rupture occurs. Studying the details of thin liquid film drainage is therefore crucial to the understanding of the coalescence process and the stability of liquid–liquid dispersions, which are of significant practical and industrial interest.

Thin liquid films have been studied extensively, reviews of which are given by Kitchener (1), Sheludko (2), Clunie *et al.* (3), Ivanov and Jain (4), Jain *et al.* (5), and Wasan and Malhotra (6). In pure systems, that is, in the absence of surface active agents, the hydrodynamics of film drainage between colliding bubbles or drops have been investigated by Chen (7), Li (8), and Klaseboer *et al.* (9), among others. However, for liquid–liquid dispersions of practical interest, surfactants, either in the form of trace impurities or additives, are very often present. The drainage of the intervening continuous phase film and hence the rate of coalescence are largely influenced by the adsorption of surfactants onto the liquid–liquid interface, which modifies the interfacial properties of the system. The presence of even small variations in the concentration of surfactant can give rise to interfacial tension gradients, which, in turn, lead to so-called Marangoni stresses that can have a significant effect on the drainage dynamics.

The effect of surfactants on the stability of films and on the coalescence of bubbles and drops has been studied by Radoëv *et al.* (10), Traykov and Ivanov (11), Sharma and Ruckenstein (12), Li (13), Danov *et al.* (14), and Valkovska *et al.* (15), among others. With the exception of the work reported in (10), wherein the surfactant concentration was assumed steady, all of the studies listed above adopt an asymptotic approach whereby the local value for the surfactant concentration is represented by the sum of the corresponding equilibrium value at steady state and a small perturbation caused by the flow. In these studies, therefore, a *quasi-steady-state* approximation is used in which all the variables in the system depend implicitly on time through the local film thickness (14, 16). Recently, however, Chesters and Bazhlekov (17) considered a dynamically evolving surfactant concentration by coupling the film evolution equation to the equation governing the transport of insoluble surfactant. In that study, a uniform concentration of surfactant was distributed onto an initially undeformed interface; interfacial deformation, brought about by axisymmetric drop approach under a small constant interaction force, caused a nonuniformity in the surfactant interfacial concentration. This, in turn, resulted in interfacial tension gradients, generating additional interfacial tangential stresses or Marangoni stresses.

In liquid–liquid systems of practical relevance, surface-active contaminants often tend to accumulate in a localized region at the interface on top of an already present background surfactant concentration (18). It is therefore important that the effect of an initially localized *nonuniform* distribution of insoluble surfactant concentration on film drainage between two drops be

[1] To whom correspondence should be addressed.

0021-9797/01 $35.00

examined in addition to the case of an initially uniform concentration of surfactant. Shen and Hartland (18) first studied this effect on local film drainage solely for the case of a bubble or a drop approaching a solid plane, but without attempting to investigate the effects of the viscosity of the fluid phase. This paper thus extends the work of Shen and Hartland (18) to account for drop–drop interactions over a wider range of viscosity ratios and to explore the possibility that Marangoni-driven local drainage may lead to film rupture by including disjoining pressure effects into the model, effects which have not been considered in (18).

The interfacial concentration gradients considered in the work of Chesters and Bazhlekov (17) arise and evolve from a uniform distribution due to interfacial deformation occurring during the film drainage process such that the Marangoni effect is a slave to the hydrodynamic processes. Here we have chosen instead to study the effect of the presence of an already present nonuniform concentration distribution imposed on a uniform background concentration on the film drainage, which we consider to occur in a region of small lateral extent, far upstream from the region in which a dimple rim may occur. The time scales for rupture, obtained from the present work, will be compared with both theoretically and experimentally determined time scales for dimpling obtained from the literature. It will be seen that the time scales for rupture due to Marangoni-driven local film drainage occur at a comparable time scale, or even in certain cases, at a faster time scale than that for the dimpling process. Therefore, we conclude that there is a possibility of film rupture due to local film drainage under the action of Marangoni stresses. In addition, we also report that the viscosity ratio plays an important role on the drainage process: A low dispersed to continuous phase viscosity ratio allows the surfactant to exhibit a stronger influence on the film drainage.

The rest of this paper is organized as follows. Section 2 is devoted to the formulation of the problem, which includes the derivation of the governing equations, the scalings most relevant to this problem, and details of the numerical procedure employed in the solution of the model equations. A discussion of the results is provided in Section 3 in which the effects of system parameters on the dynamics of the drainage process are examined. These parameters include the surface Péclet number, which characterizes Marangoni stresses and surface diffusion, a Hamaker constant, which characterizes van der Waals forces, the background surfactant concentration, and the viscosity ratio. Finally, concluding remarks are provided in Section 4.

2. MATHEMATICAL FORMULATION AND SOLUTION METHODOLOGY

We begin the problem formulation by listing all the assumptions which have been adopted to simplify the mathematical model to be solved:

1. The interfaces between the dispersed phases and the draining film are axisymmetric.

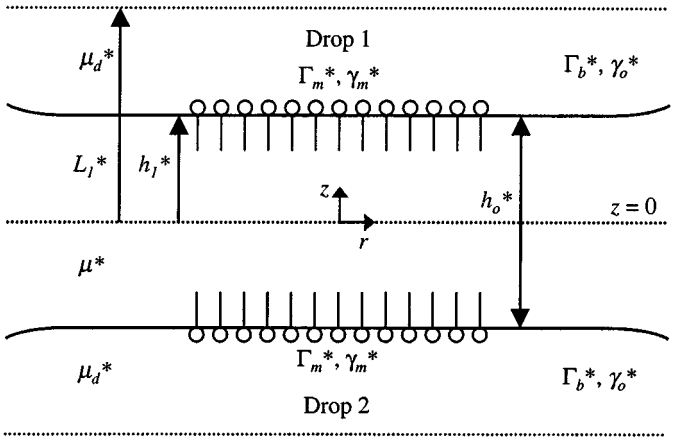

FIG. 1. Schematic representation of the local drainage region between two drops.

2. Since a very small and localized region of the film is to be examined, an initially plane-parallel film is assumed as shown in Fig. 1, i.e., the film is of initially uniform thickness, h_o^*; the asterisk signifies a dimensional quantity. As a consequence of the extremely small values of the film thicknesses involved, the associated Reynolds and Bond numbers are small, and hence inertial as well as gravitational forces are negligible. Lubrication theory (the balance of viscous forces with the pressure gradient in flows where inertial forces are negligible) therefore applies.

3. The effects of the drainage within the local region considered are so localized that these effects are not affected by the drainage in the entire film. Outside this region, therefore, the surfactant concentration and the film thickness remain unaltered during the period in which local drainage occurs (18).

4. The dispersed and the continuous phases are both assumed to be incompressible and Newtonian. The drops are assumed to be initially spherical, where R_i^* is the radius of drop i.

5. In the drop, the velocity and the velocity gradient approach zero at some distance from the interface, L_i^*, which is the characteristic circulation length of viscous penetration in drop i given by (19)

$$L_i^* = \frac{h_o^* R_i^*}{R_o^*}. \qquad [1]$$

In [1], R_o^* is the initial rim radius of the film outside the local drainage region at which point the dimple rim would occur if the entire intervening continuous-phase film between the drop had been considered. Assuming that L_i^* is small compared to the drop radius, R_i^*, then the z-component of the pressure distribution in the drop is negligible compared to the radial component.

6. Since the film is thin with respect to the region in which the hydrodynamic interaction of the drops occurs, which in turn is small compared to the drop radius (i.e., $h_o^* \ll R_o^* < R_i^*$), the effect of the difference in drop radii on the curvature of the film is negligible. It is possible then to assume symmetry relative

to the plane $z^* = 0$; the drainage of the film between drops of different sizes R_1^* and R_2^* is equal to that between equal-sized drops with an equivalent radius R^* (9, 20), where

$$\frac{1}{R^*} = \frac{1}{2}\left(\frac{1}{R_1^*} + \frac{1}{R_2^*}\right). \quad [2]$$

7. Because of the above assumption of symmetry at the plane $z^* = 0$, it is also possible to assume that the interfacial properties of the two surfaces are the same (14). Thus $\gamma_1^* = \gamma_2^* = \gamma^*$, where γ_i^* is the interfacial tension at the interface of drop i and γ^* is the interfacial tension which is a function of the interfacial concentration of insoluble surfactant, Γ^*.

8. A surfactant monolayer of prescribed initial concentration profile is imposed axisymmetrically at the interface between the dispersed and continuous phases about the center of the local contamination region; the surfactant is assumed to be present in dilute concentrations. The surfactant is also assumed to be insoluble in both the dispersed and the continuous phases. The insolubility of the surfactant in the dispersed and the continuous phases is approximated at low concentration of surfactants when the partition coefficient favors adsorption of the surfactant at the interface (21). This is also a good approximation when diffusion of surfactant between the bulk and the interface occurs on a time scale much larger than the time scales at which film drainage occurs (17). Steric hindrances and changes in the dilational and shear interfacial viscosities due to the presence of surfactant at the interface are neglected.

9. Disjoining pressure effects are incorporated into the model by taking into account van der Waals forces only; electric double layer forces are neglected.

2.1. Governing Equations

The problem is formulated in dimensionless variables whose relations to the dimensional variables are given as

$$\begin{aligned} r &\equiv \frac{r^*}{R_o^*}, \quad z \equiv \frac{z^*}{h_o^*}, \quad h \equiv \frac{h^*}{h_o^*}, \quad p \equiv \frac{h_o^*}{S^*}p^*, \\ t &\equiv \frac{\epsilon S^*}{\mu^* R_o^*}t^*, \quad v_r \equiv \frac{\mu^*}{\epsilon S^*}v_r^*, \quad \lambda \equiv \frac{\mu_d^*}{\mu^*}, \\ R_i &\equiv \frac{R_i^*}{R_o^*}, \quad \Gamma \equiv \frac{\Gamma^*}{\Gamma_m^*}, \quad \gamma \equiv \frac{(\gamma^* - \gamma_m^*)}{S^*}, \end{aligned} \quad [3]$$

where h is the film thickness, t is the time, p is the pressure in the film, and p_i is the pressure of drop i; μ^* and μ_d^* are the viscosities of the continuous and dispersed phases, respectively; v_r and v_{r_i} are the radial velocities in the film and in the dispersed phase i, respectively. ϵ is a small parameter describing the ratio of the axial to radial length scales, i.e., $\epsilon \equiv h_o^*/R_o^*$. A spreading parameter, $S^* = \gamma_o^* - \gamma_m^*$, is defined such that γ_o^* and γ_m^* represent the interfacial tension corresponding to the least contaminated part of the interface and that of the interfacial region saturated with surfactant at concentration, Γ_m^*, respectively.

Given assumptions 1–9 listed above, the Navier–Stokes equations reduce to the lubrication equations. These are given by

$$\frac{\partial p}{\partial r} = \frac{\partial^2 v_r}{\partial z^2} \quad [4]$$

for the film and

$$\frac{\partial p_i}{\partial r} = \lambda \frac{\partial^2 v_{r_i}}{\partial z^2} \quad [5]$$

for the drops.

Integration of Eq. [5] and application of the condition that the velocity and the velocity gradient in the drop approach zero at a characteristic length, L_i, yields an expression for the radial velocity in the dispersed phase given by

$$v_{r_i} = \frac{[z - (h_i \pm R)]^2}{2\lambda}\frac{\partial p_i}{\partial r}, \quad [6]$$

where $h_i = h/2$ is that part of the film thickness between drop i and the plane $z = 0$ (see Fig. 1). The addition sign corresponds to $i = 1$ and the subtraction sign corresponds to $i = 2$.

The tangential shear stress balance at the interfaces expressed by

$$\left.\frac{\partial v_r}{\partial z}\right|_{z=h_1} - \lambda \left.\frac{\partial v_{r_1}}{\partial z}\right|_{z=h_1} = \frac{\partial \gamma}{\partial r}, \quad [7]$$

$$\lambda \left.\frac{\partial v_{r_2}}{\partial z}\right|_{z=h_2} - \left.\frac{\partial v_r}{\partial z}\right|_{z=h_2} = \frac{\partial \gamma}{\partial r} \quad [8]$$

can be used to recast the drop velocities v_{r_1} and v_{r_2} in terms of $\partial p/\partial r$. At the interfaces ($z = h_i$), therefore,

$$v_{r_{int}} = \frac{R}{2\lambda}\frac{\partial \gamma}{\partial r} - \frac{hR}{4\lambda}\frac{\partial p}{\partial r}, \quad [9]$$

where $v_{r_{int}}$ is the radial component of the interfacial velocity.

Integration of Eq. [4], taking into account symmetry at the plane $z = 0$, and demanding continuity of the velocity at both drop interfaces

$$v_r|_{z=h_i} = v_{r_{int}} \quad (i = 1, 2), \quad [10]$$

yields an expression for the radial film velocity:

$$v_r = \frac{z^2}{2}\frac{\partial p}{\partial r} - \frac{h}{4\lambda}\left(\frac{\lambda h}{2} + R\right)\frac{\partial p}{\partial r} + \frac{R}{2\lambda}\frac{\partial \gamma}{\partial r}. \quad [11]$$

The kinematic boundary condition is given by

$$\frac{\partial h}{\partial t} = -\frac{1}{r}\frac{\partial}{\partial r}(rh\bar{v}_r), \quad [12]$$

where $\bar{v}_r$ is the mean radial velocity in the film. Combination of Eqs. [9], [11], and [12] results in an evolution equation for the

film expressed by

$$\frac{\partial h}{\partial t} = \frac{1}{12r}\frac{\partial}{\partial r}\left(rh^3\frac{\partial p}{\partial r}\right) - \frac{1}{r}\frac{\partial}{\partial r}(rhv_{r_{int}}). \quad [13]$$

The normal stress balance giving the excess pressure in the film relative to the bulk pressure consists of the pressure difference in the drop (the Laplace pressure), the pressure associated with the local interfacial curvature, and the disjoining pressure taking into account the van der Waals interaction (22). We thus write

$$p^* = \frac{2\gamma^*}{R^*} - \frac{\gamma^*}{2}\left[\frac{1}{r^*}\frac{\partial}{\partial r^*}\left(r^*\frac{\partial h^*}{\partial r^*}\right)\right] + \left(\Phi^*_\infty + \frac{B^*}{h^{*^m}}\right), \quad [14]$$

where Φ^*_∞ is the van der Waals interaction potential per unit volume of a semi-infinite liquid film in the limit of approaching the liquid–liquid interface, B^* is the Hamaker constant, and m is a parameter.

By definition,

$$\Phi_\infty \equiv \frac{h^*_o}{S^*}\Phi^*_\infty; \quad B \equiv \frac{B^*}{S^* h^{*^{m-1}}_o}. \quad [15]$$

Insertion of the scalings defined by [3] into Eq. [14], and assuming that $\epsilon \ll 1$, yields an expression for the dimensionless pressure in the film:

$$p = \frac{2}{R}\frac{\epsilon\gamma^*_m}{S^*} - \frac{1}{2}\frac{\epsilon^2\gamma^*_m}{S^*}\left[\frac{1}{r}\frac{\partial}{\partial r}\left(r\frac{\partial h}{\partial r}\right)\right] + \left(\Phi_\infty + \frac{B}{h^m}\right). \quad [16]$$

Below we consider two cases: $S^* = \epsilon^2\gamma^*_m$, that is, a spreading coefficient of small magnitude, appropriate for trace amounts of surfactant, and $S^* \sim O(1)$; we shall focus, however, on the first case for practical reasons.

The interfacial concentration of the insoluble surfactant is allowed to evolve dynamically and is governed by the convective–diffusion equation

$$\frac{\partial \Gamma^*}{\partial t^*} + \frac{1}{r^*}\frac{\partial}{\partial r^*}(r^* v^*_{r_{int}}\Gamma^*) = D^*_s\left[\frac{1}{r^*}\frac{\partial}{\partial r^*}\left(r^*\frac{\partial \Gamma^*}{\partial r^*}\right)\right], \quad [17]$$

where D^*_s is the surface diffusivity. In dimensionless terms, the surfactant transport equation becomes

$$\frac{\partial \Gamma}{\partial t} + \frac{1}{r}\frac{\partial}{\partial r}(r v_{r_{int}}\Gamma) = \frac{1}{\mathrm{Pe}_s}\left[\frac{1}{r}\frac{\partial}{\partial r}\left(r\frac{\partial \Gamma}{\partial r}\right)\right], \quad [18]$$

in which the surface Péclet number, Pe_s, is defined as

$$\mathrm{Pe}_s = \frac{S^* h^*_o}{\mu^* D^*_s}, \quad [19]$$

which represents the ratio of transport by Marangoni stresses to that by surface diffusion. Assuming dilute concentrations of insoluble surfactant, a linear surface equation of state for the interfacial tension was adopted as a relationship between the interfacial tension and the local surfactant interfacial concentration:

$$\gamma^* = \gamma^*_o - \left(\frac{\partial \gamma^*}{\partial \Gamma^*}\right)\Gamma^*. \quad [20]$$

Inserting the scalings into Eq. [20] and noting that $\Gamma^* = \Gamma^*_m$ when $\gamma^* = \gamma^*_m$ yields the dimensionless equation of state

$$\gamma = 1 - \Gamma. \quad [21]$$

2.2. Initial and Boundary Conditions

In order to solve the film and surfactant evolution equations, we impose the initial conditions

$$h(r, 0) = 1, \quad [22]$$

$$\Gamma|_{t=0} = (1 - \Gamma_b)\frac{1 - \tanh\left(\frac{r-\xi_o}{\xi_1}\right)}{1 - \tanh\left(-\frac{\xi_o}{\xi_1}\right)} + \Gamma_b, \quad [23]$$

where Γ_b is the background concentration of surfactant, ξ_o denotes the value of r for which $\Gamma = \Gamma_b$, and ξ_1 controls the steepness of the initial concentration distribution. In addition, the necessary boundary conditions are

$$\left.\frac{\partial h}{\partial r}\right|_{r=0} = 0, \quad [24]$$

$$\left.\frac{\partial^3 h}{\partial r^3}\right|_{r=0} = 0, \quad [25]$$

$$h|_{r=r_\infty} = 1, \quad [26]$$

$$\left.\frac{\partial h}{\partial r}\right|_{r=r_\infty} = 0, \quad [27]$$

$$\left.\frac{\partial \Gamma}{\partial r}\right|_{r=0} = 0, \quad [28]$$

$$\Gamma|_{r=r_\infty} = \Gamma_b, \quad [29]$$

where r_∞ is a radial distance far from the region where local film drainage takes place. The boundary condition given by Eq. [25] is a consequence of the requirement that $\partial p/\partial r = 0$ at $r = 0$ (23).

2.3. Numerical Scheme

Equation [18] and the combination of Eqs. [13] and [16], which govern the spatio-temporal evolution of the continuous film thickness and surfactant interfacial concentration are a coupled pair of fourth-order nonlinear parabolic partial differential equations. These evolution equations were solved numerically subject to the initial and boundary conditions [22]–[29] using the Numerical Method of Lines (24) utilizing fourth-order centered differences for the discretization of spatial derivatives and

Gear's method in time (25). Values of $R = 4$ (19), $\xi_o = 3$, and $\xi_1 = 0.6$ were used for all the simulations reported in the present work. Other choices of initial surfactant distribution yielded only quantitatively different results. The parameter m associated with the van der Waals interaction force was set equal to 3 while the Hamaker constant (7, 22), B^*, equaled 10^{-21} J. Numerical solutions were obtained for $0.1 \le \mathrm{Pe}_s \le 100$, $0.1 \le \lambda \le 10$, $0 \le \Gamma_b \le 0.3$, and $1 \le B \le 1 \times 10^{-3}$, over spatial domains of maximum length 25 dimensionless units for times of order 100 dimensionless seconds using up to 1000 grid points; convergence was achieved upon mesh refinement. In the case of film rupture, the computations were halted when the minimum film thickness was approximately 0.1 because of the difficulty in resolving accurately the increasingly singular spatial derivatives in the rupture region. The rupture times quoted therefore correspond to the time at which the computations were halted.

3. RESULTS AND DISCUSSION

For practical reasons, this paper will largely focus on the effects of a trace amount of nonuniform surfactant imposed at the drop interface. However, a similarity analysis is conducted for the general case where the surfactant concentration is not limited to a small amount. Section 3.1 is devoted to this study. In Section 3.2, a parametric study is then carried out to elucidate the influence of various parameters on the interfacial spreading of the insoluble surfactant and on the local film drainage process in the limit where only trace amounts of surfactant are present. The parameters which are studied are the viscosity ratio, λ, the surface Péclet number, Pe_s, and the background surfactant concentration, Γ_b. In addition, the effect of van der Waals forces on film rupture is investigated. The development of film and concentration profiles for typical parameter values are reported in Section 3.2.1. Section 3.2.2 focuses on the effect of λ on local film drainage. In Section 3.2.3, the effect of Γ_b on the spreading of surfactant at the interface is studied; this is followed by Section 3.2.4 wherein the effect of Pe_s, representing the ratio of surfactant transport by Marangoni stresses to that by surface diffusion, is discussed. Finally, film rupture under the influence of van der Waals interaction forces is considered in Section 3.2.5.

3.1. Marangoni-Dominated Spreading: $S^* \sim O(1)$

In this section, we present the case where the spreading coefficient is large, i.e., $S^* \sim O(1)$. Although this is not the practically relevant case, we have included this section for completeness and also to validate the predictions of the numerical scheme through a comparison with similarity solutions. Only a brief outline of the derivation of the similarity analysis will be presented here; the full derivation is described in the Appendix.

If only Marangoni forces were present such that $1/\mathrm{Pe}_s \to 0$ and $\epsilon^2\gamma_m^*/S^* \to 0$, then Eqs. [13] and [18] can be simplified to

$$\frac{\partial h}{\partial t} = \frac{1}{r}\frac{\partial}{\partial r}\left[rh\left(\frac{R}{2\lambda}\frac{\partial \Gamma}{\partial r}\right)\right], \qquad [30]$$

$$\frac{\partial \Gamma}{\partial t} = \frac{1}{r}\frac{\partial}{\partial r}\left[r\Gamma\left(\frac{R}{2\lambda}\frac{\partial \Gamma}{\partial r}\right)\right]. \qquad [31]$$

Global conservation of the mass of surfactant, M, also requires

$$M = 2\pi \int_0^\infty r\Gamma \, \mathrm{d}r. \qquad [32]$$

Following Jensen and Grotberg (26), we then introduce into Eqs. [30]–[32] the set of similarity scalings

$$h(r,t) = H(\xi,\tau), \quad \xi = \frac{r}{\xi_s t^a},$$
$$\Gamma(r,t) = \frac{\xi_s^2 G(\xi,\tau)}{t^b}, \quad t = \tau, \qquad [33]$$

where the position of the surfactant leading edge is located at $\xi = 1$ via rescaling by the parameter ξ_s (see Appendix). In these transformed coordinates, Eqs. [30]–[32] are rendered time-independent when $2a + b - 1 = 0$ and $2a - b = 0$ for a finite mass of surfactant, M. Thus $a = \frac{1}{4}$ and $b = \frac{1}{2}$, implying that the surfactant leading edge advances as $t^{\frac{1}{4}}$.

It can then be shown that the similarity solution for the evolution of the film thickness is

$$H = \frac{\delta(1-\xi)}{2} - \Theta(1-\xi) + 1, \qquad [34]$$

where $\delta(1-\xi)$ is the Dirac delta function and $\Theta(1-\xi)$ is the Heaviside function. Behind the surfactant leading edge ($\xi < 1$), therefore, the film thins such that the film profile is nearly horizontal, tending to $H = 0$. At the surfactant leading edge ($\xi = 1$), $H = \infty$, indicating a sharp discontinuity or a frontal shocklike structure of infinite height in the film profile. In front of the shock ($\xi > 1$), the profile tends to its undisturbed position, $H = 1$. Equation [34] is used as a limiting case to validate the predictions of the numerical scheme.

Figures 2a and 2b show the film evolution in the original coordinate system and in the transformed coordinates respectively. These profiles were obtained via numerical solutions of Eqs. [13] and [18] with $\epsilon^2\gamma_m^*/S^* = 10^{-4}$ and $\mathrm{Pe}_s = 1000$. Upstream of the shock, the film becomes increasingly flat, tending toward $H = 0$, whereas downstream, the film remains undisturbed, in agreement with the similarity solution presented above. The growing shocklike front is also captured by the Dirac delta function in the similarity analysis. The position of the shock in Fig. 2b tends toward the theoretical shock position $\xi = 1$ with time. The similarity solution therefore provides a reasonable approximation to the numerical solution over the majority of the spatial domain. We now detail results of the study for a more relevant case, that is, the case where trace quantities of surfactant are present at the interface.

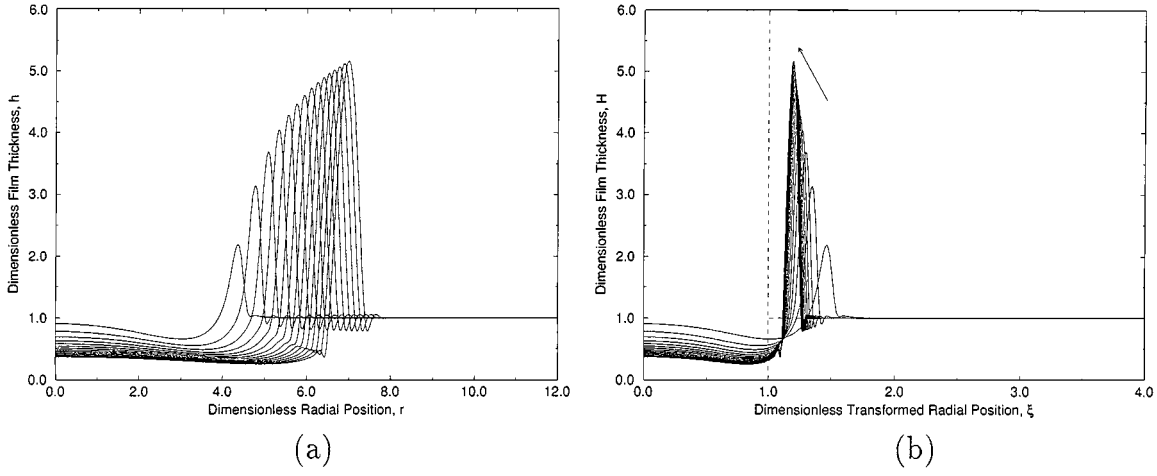

FIG. 2. Profiles for the evolution of the film thickness in (a) the original untransformed coordinates and in (b) similarity variables for 15 equal time steps up to $t = 8$ with $\lambda = 1$, $\mathrm{Pe}_s = 1000$, $\Gamma_b = 0$, $B = 1 \times 10^{-3}$, and $\epsilon^2\gamma_m^*/S^* = 10^{-4}$. (The dashed line is the similarity solution, indicating the theoretical position of the frontal shock that the profiles should tend toward over a large period of time; the arrow indicates the direction of increasing time.)

3.2. Trace Amounts of Surfactant: $S^* \sim O(\epsilon^2)$

In the limit of very small quantities of surfactant, the spreading pressure, S^*, is small. By approximating $S^* = \epsilon^2\gamma_m^*$, the scaling for the pressure can now be rewritten as

$$p \equiv \frac{h_o^*}{\epsilon^2\gamma_m^*}\, p^*, \qquad [35]$$

and therefore the dimensionless pressure gradient in the film now reads

$$\frac{\partial p}{\partial r} = -\frac{1}{2}\frac{\partial}{\partial r}\left[\frac{1}{r}\frac{\partial}{\partial r}\left(r\frac{\partial h}{\partial r}\right)\right] - \frac{mB}{h^{m+1}}\left(\frac{\partial h}{\partial r}\right). \qquad [36]$$

The rest of this paper reports an investigation of various system parameters in this limit.

3.2.1. Development of film and concentration profiles. Figures 3a and 3b show typical spatio-temporal development of the film and the surfactant interfacial concentration, respectively, for the following parameter values: $\lambda = 1$, $\mathrm{Pe}_s = 10$, $\Gamma_b = 0$, and $B = 10^{-2}$, from $t = 0$ to 8.62 in 15 equal time steps. Large gradients in surfactant concentration arising from the initially nonuniform concentration distribution imposed on the film give rise to surface tension gradients and hence Marangoni shear stresses, which are pronounced near the flow origin. The film thickness thins in that region in order for viscous drag to balance interfacial stresses and, to satisfy mass conservation, the film thickens at the surfactant leading edge. An outspreading fluid mechanical wave, similar to the structure

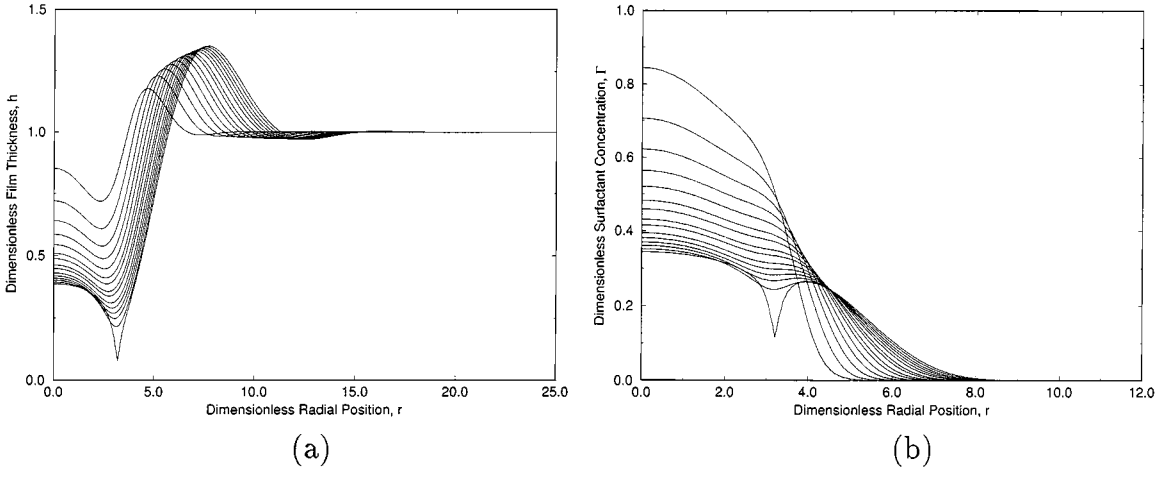

FIG. 3. Film thickness (a) and surfactant concentration (b) profiles for 15 equal time steps up to $t = 8.62$ with $\lambda = 1$, $\mathrm{Pe}_s = 10$, $\Gamma_b = 0$, and $B = 1 \times 10^{-2}$.

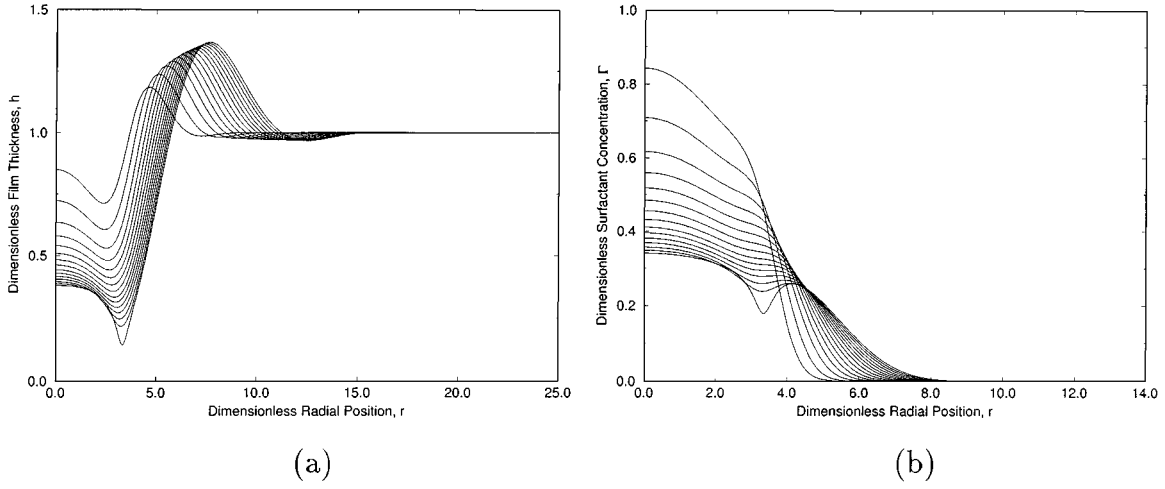

FIG. 4. Film thickness (a) and surfactant concentration (b) profiles for 15 equal time steps up to $t = 0.88$ for $\lambda = 0.1$; the other parameter values are $\mathrm{Pe}_s = 1$, $\Gamma_b = 0$, and $B = 1 \times 10^{-2}$.

previously calculated by Shen and Hartland (18) and Jensen and Grotberg (26), is therefore generated. The surfactant concentration profiles gradually become flatter as the surfactant concentration decreases to its background value, which, in this case, is zero.

The thinning is so rapid and severe that van der Waals interactions become significant and the film can be seen tending toward rupture at the last time step shown in Fig. 3. van der Waals forces expel both liquid and surfactant from the region of film rupture, giving rise to a sharp depletion in surfactant in that region. As a result, a local interfacial tension gradient arises, which causes the transport of surfactant and liquid back into the rupture region, thereby acting to replenish the film and to reduce film thinning in opposition to van der Waals forces. In this example, however, it is evident that the Marangoni backflow into the film rupture region is insufficient to counteract the van der Waals attraction and thus the film ruptures.

3.2.2. Effect of the viscosity ratio. The local film drainage was studied for three viscosity ratios, $\lambda = 0.1$, 1.0, and 10.0, with the rest of the parameter values kept constant at $\mathrm{Pe}_s = 1$, $B = 1 \times 10^{-2}$, and $\Gamma_b = 0$. The evolution of the film thickness and surfactant concentration profiles for each of these viscosity ratios can be seen in Figs. 4–6. The influence of the surfactant on film thinning and rupture is seen to diminish as the viscosity ratio increases, as evidenced by the longer times that are required for the film to drain to a specified film thickness (see also Fig. 7). This is to be expected since the spreading of surfactant along the interface is much slower when the viscosity ratio is large because the increased resistance by the dispersed phase

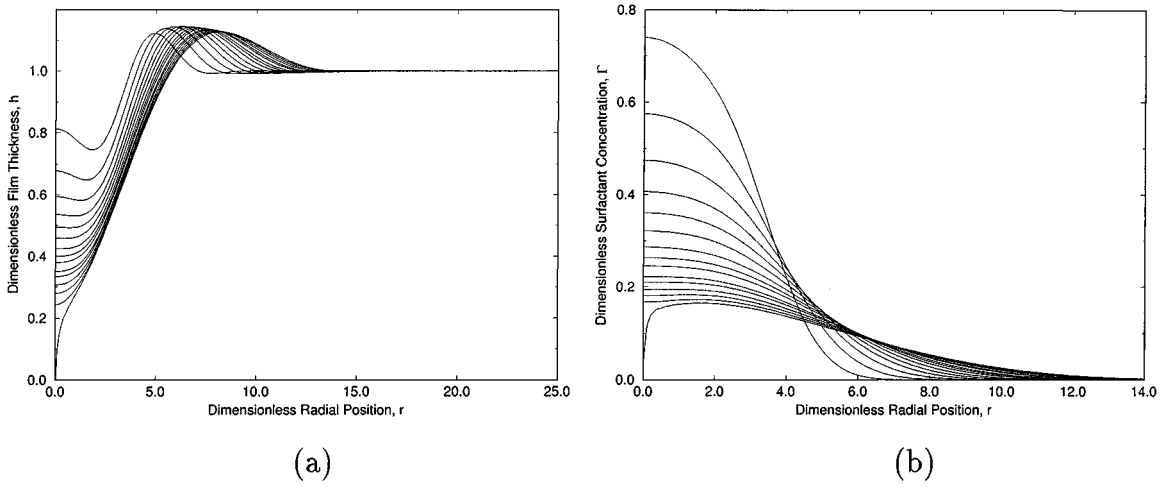

FIG. 5. Film thickness (a) and surfactant concentration (b) profiles for 15 equal time steps up to $t = 8.924$ for $\lambda = 1$; the other parameter values are $\mathrm{Pe}_s = 1$, $\Gamma_b = 0$, and $B = 1 \times 10^{-2}$.

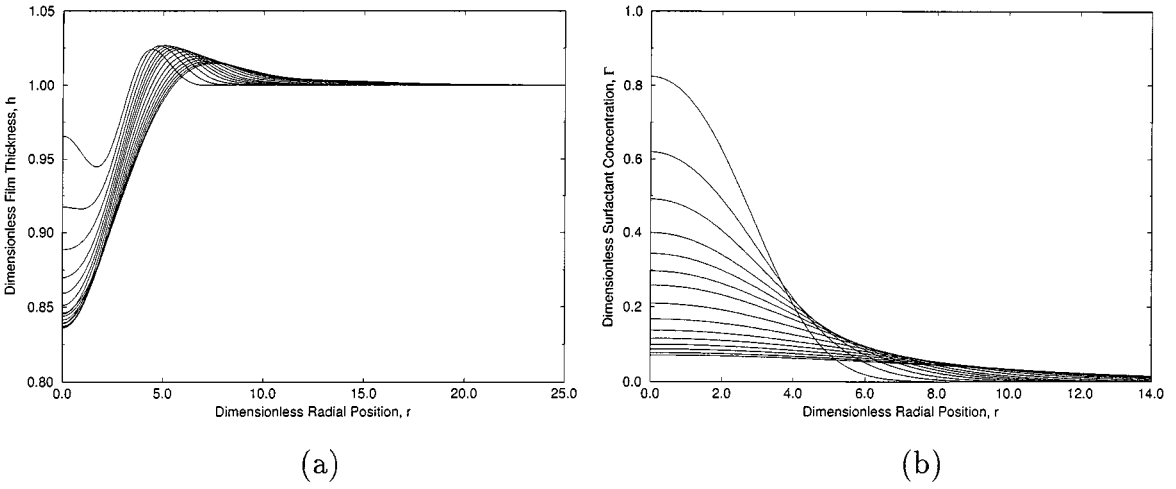

FIG. 6. Film thickness (a) and surfactant concentration (b) profiles at times $t = 1.0$, 2.0, 3.0, 4.0, 5.0, 6.0, 7.0, 9.0, 12.0, 15.0, 18.0, 21.0, 24.0, 27.0, and 30.0 for $\lambda = 10$; the other parameter values are $\mathrm{Pe}_s = 1$, $\Gamma_b = 0$, and $B = 1 \times 10^{-2}$.

reduces the interfacial mobility. This is illustrated in Fig. 8, which shows the surfactant spreading rate along the interface, defined by the rate of advancement of the radial position at which the surfactant concentration decreases to zero, or the background surfactant concentration. It can be seen that the effect of viscosity ratios on the spreading rate becomes increasingly evident as Marangoni forces become dominant, as demonstrated by the surface Péclet number, Pe_s.

The retardation of the interfacial velocity due to Marangoni stresses by the viscous dispersed phase also explains why the point of rupture is closer to the center for increasing viscosity ratios. Film rupture occurs approximately at a radial position $r = 3.36$ for $\lambda = 0.1$, whereas for $\lambda = 1$ rupture occurs at the center as shown in Figs. 4a and 5a respectively. For the case of $\lambda = 10$ (Fig. 6a), the film does not thin sufficiently for van der Waals forces to act before rethickening of the film occurs as hydrodynamic effects attempt to recover the drop curvature, and hence rupture does not occur. In addition, less flattening of the film is observed with increasing viscosity ratios, indicating an increased resistance to film deformation, which may have arisen due to Marangoni stresses. The decreasing magnitude in the height of the outspreading wave is also a consequence of the decreasing deformability of the interface with high viscosity ratios.

A comparison of Figs. 4b and 5b reveals that the high surfactant spreading rates associated with low viscosity ratios result in a slight flattening of the concentration profile near the thinning region upstream of the thickened front. This occurs due to rapid transport of surfactant and liquid away from the vicinity

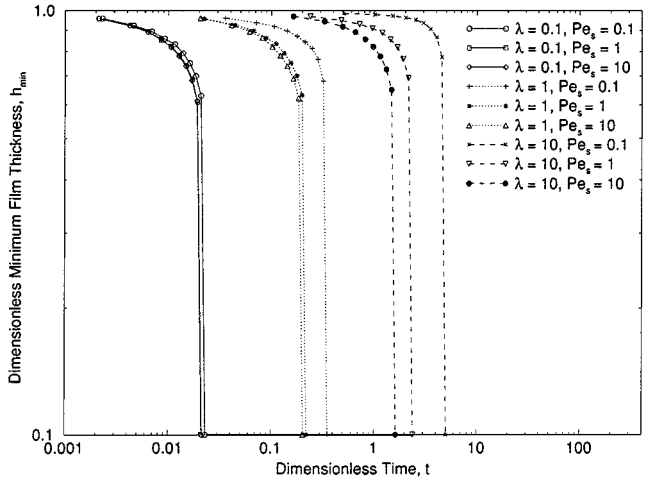

FIG. 7. Variation of minimum film thickness with time as a function of the viscosity ratio, λ, and the surface Péclet number, Pe_s. The other parameter values are $\Gamma_b = 0$ and $B = 1$.

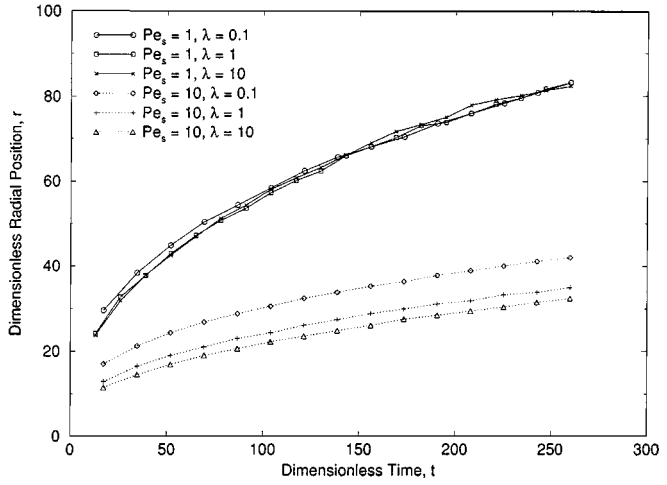

FIG. 8. The effect of varying the viscosity ratio, λ, on the surfactant spreading rate for $\mathrm{Pe}_s = 1$ and $\mathrm{Pe}_s = 10$. The other parameter values are $\Gamma_b = 0$ and $B = 0$.

of the flow origin, which gives rise to rapid thinning and sharp depressions in the film profiles. As a consequence, a small indentation in the surfactant profile is observed to form a short distance downstream of the thinning region for $\lambda = 0.1$ in Fig. 4b. This is absent for larger viscosity ratios for which the spreading rate is lower. In the region of the indentation, there arises a small positive concentration gradient that creates a small retardation effect to the flow of surfactant outward. The indentation effect becomes more evident for higher Pe_s (not shown).

We shall return to Fig. 7 in Section 3.2.4, wherein we examine the effect of Pe_s on the dynamics.

3.2.3. Effect of background surfactant concentration. Shen and Hartland (18) studied the effect of background surfactant concentration in their system on the drainage of a liquid film formed between a bubble approaching a solid plane. They found little significance of the background concentration on the thinning process in the initial stages of film thinning as the background concentration is small compared to the additional surfactant concentration imposed on it. However, as the film thickness approached its minimum, Shen and Hartland observed film recovery as the film began to thicken once again. Similar observations were made in the present work. Figure 9 shows the minimum film thickness as a function of time for various background concentrations. It can be seen that as the background concentration is increased, the onset of flow reversal occurs earlier and at a higher minimum film thickness. This is consistent with Shen and Hartland's observations that the cleaner the interface, the smaller the minimum film thickness and the later the onset of film recovery (18). As in (18), this observation can be explained by the presence of an interfacial tension gradient arising due to the background surfactant, which opposes the outward flow of the film. It is also instructive to examine the concentration profiles for various viscosity ratios where background surfactant is present; these are shown in Figs. 10a–10c. In all cases, the surfactant concentration can be seen to spread until the background value is reached. A comparison of Figs. 4b and 10a for clean and contaminated interfaces, respectively, and the same viscosity ratio, reveals the formation of an additional kink in Fig. 10a immediately upstream of the region in which the surfactant concentration decreases to its background value; this feature was independent of the size of the computational domain. This additional kink in the concentration arises due to the presence of the background surfactant, which creates a positive concentration gradient that opposes the flow in the film leading to flow reversal. For higher viscosity ratios (Figs. 10b and 10c), this effect becomes less and less pronounced.

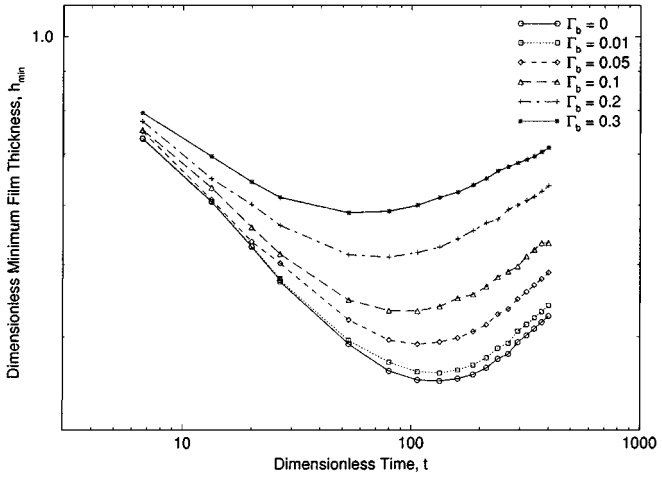

FIG. 9. The effect of varying the background surfactant concentration, Γ_b, on the minimum film thickness. The other parameter values are $\lambda = 10$, $\mathrm{Pe}_s = 10$, and $B = 0$.

3.2.4. Effect of the surface Péclet number. The surface Péclet number, Pe_s, represents a ratio of surfactant transport by Marangoni stresses to that by surface diffusion. In this section, we examine the effect of varying Pe_s on the flow characteristics in the absence of van der Waals forces and background concentration effects. A range of $0.1 < \mathrm{Pe}_s < 100$ is studied, which represents the range between diffusive and convective spreading. Since we examine the case where only trace amounts of surfactant are present, values of Pe_s above 10 are impractical. However, we have included the case where $\mathrm{Pe}_s = 100$ to further elucidate the effects of spreading due to Marangoni convection.

Figures 11a–11d show the surfactant concentration profiles for various Pe_s values from the limit of surface-diffusion-dominated surfactant transport, $\mathrm{Pe}_s = 0.1$, to that where Marangoni convection is the dominant driving mechanism, $\mathrm{Pe}_s = 100$. The diffusive time scale, T_d, is given by

$$T_d = \frac{R_o^{*^2}}{D_s}, \qquad [37]$$

while that for Marangoni-driven spreading, T_c, is

$$T_c = \frac{\mu^* R_o^*}{\epsilon S}, \qquad [38]$$

from which it follows that $T_d = \mathrm{Pe}_s T_c$.

At low Pe_s, it can thus be seen that $T_d \ll T_c$ and thus surface diffusion acts quickly to distribute the surfactant along the interface with little disturbance caused to the film. Any interfacial tension gradients are therefore diminished owing to the dilution of surfactant, thereby reducing any spreading effects due to Marangoni stresses. This is seen in Figs. 11a and 11b for $\mathrm{Pe}_s = 0.1$ and 1 as demonstrated by the short times that are required for the concentration profile to even out at time scales suggested by Eq. [37]. In these cases of low Pe_s, the film begins to thicken again, as seen in Fig. 6a, when the interfacial tension gradients are diminished (Fig. 6b) since there are no longer sufficient interfacial stresses to overcome the hydrodynamic effects attempting to recover the drop curvature.

When Pe_s is sufficiently large [$\mathrm{Pe}_s \gg O(1)$], there are substantial interfacial tension gradients which give rise to

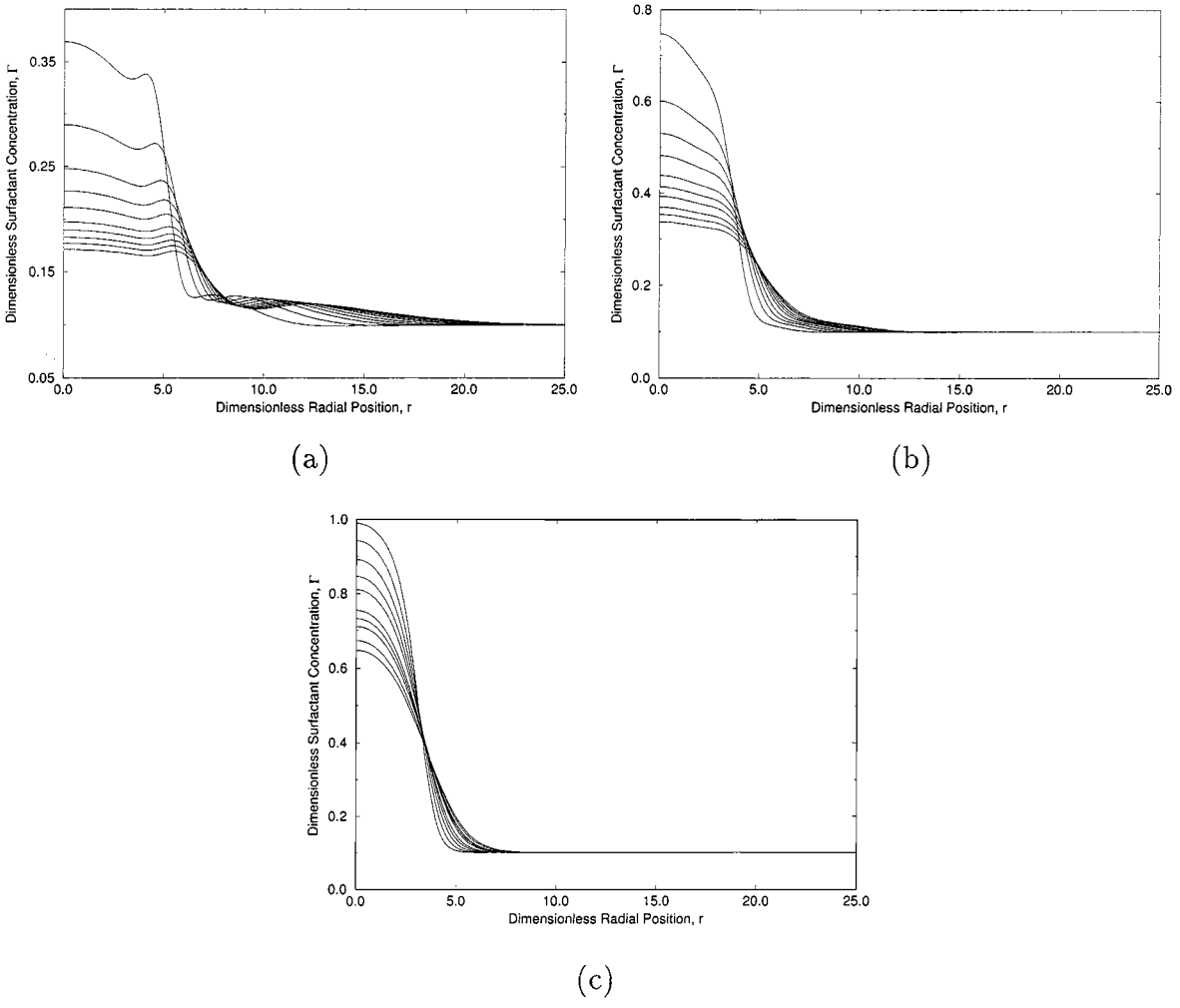

FIG. 10. The effect of varying viscosity ratio on surfactant concentration profiles in the presence of background surfactant concentration, $\Gamma_b = 0.1$: (a) $\lambda = 0.1$, (b) $\lambda = 1$, and (c) $\lambda = 10$ up to $t = 10$ in equal time steps. The other the parameter values are $\mathrm{Pe}_s = 10$ and $B = 0$.

Marangoni-dominated transport, on time scales which are shorter than those associated with diffusional processes, given by Eq. [37]. The effect of Pe_s on the spreading process is summarized in Fig. 12, which clearly shows that the surfactant spreading rate along the interface decreases as Pe_s becomes large. This trend has also been observed by Gaver and Grotberg (27) in their study of surfactant spreading on thin viscous films within the context of surfactant replacement therapy.

It is also of interest to examine the effect of Pe_s on the film profiles. Examination of Fig. 7, which depicts the influence of Pe_s on film thinning, reveals that the effect of Pe_s on the spreading rate becomes more evident at higher viscosity ratios as seen in Figs. 7 and 8: As Pe_s is increased, there is a tendency for the film to drain faster, driven by Marangoni convection.

3.2.5. Effect of van der Waals forces on film rupture. For very small length scales (of approximately 1000 Å), intermolecular forces such as van der Waals (and for much thinner films, electric double layer forces) become significant and dominate the final stages of the film drainage process as the film thins to very small thicknesses. The van der Waals force creates a negative contribution to the disjoining pressure, resulting in the destabilization of the film and thus promoting rupture, whereas the electric double layer force provides a positive contribution, stabilizing the film against rupture. In this paper, we have only analyzed the effect of van der Waals forces on the drainage and rupture process.

We have shown in Section 3.2.1 that Marangoni forces alone are insufficient to induce the film to thin to zero thickness; this is in agreement with previous studies (26). However, the film does thin sufficiently due to these forces to thicknesses at which van der Waals attraction can cause the film to become unstable and proceed toward rupture as seen in Figure 3a. On the other hand, when van der Waals forces are strong, any slight thinning of the film due to the Marangoni effect will lead to rupture of the film. Figure 13a illustrates rapid thinning and rupture of the film

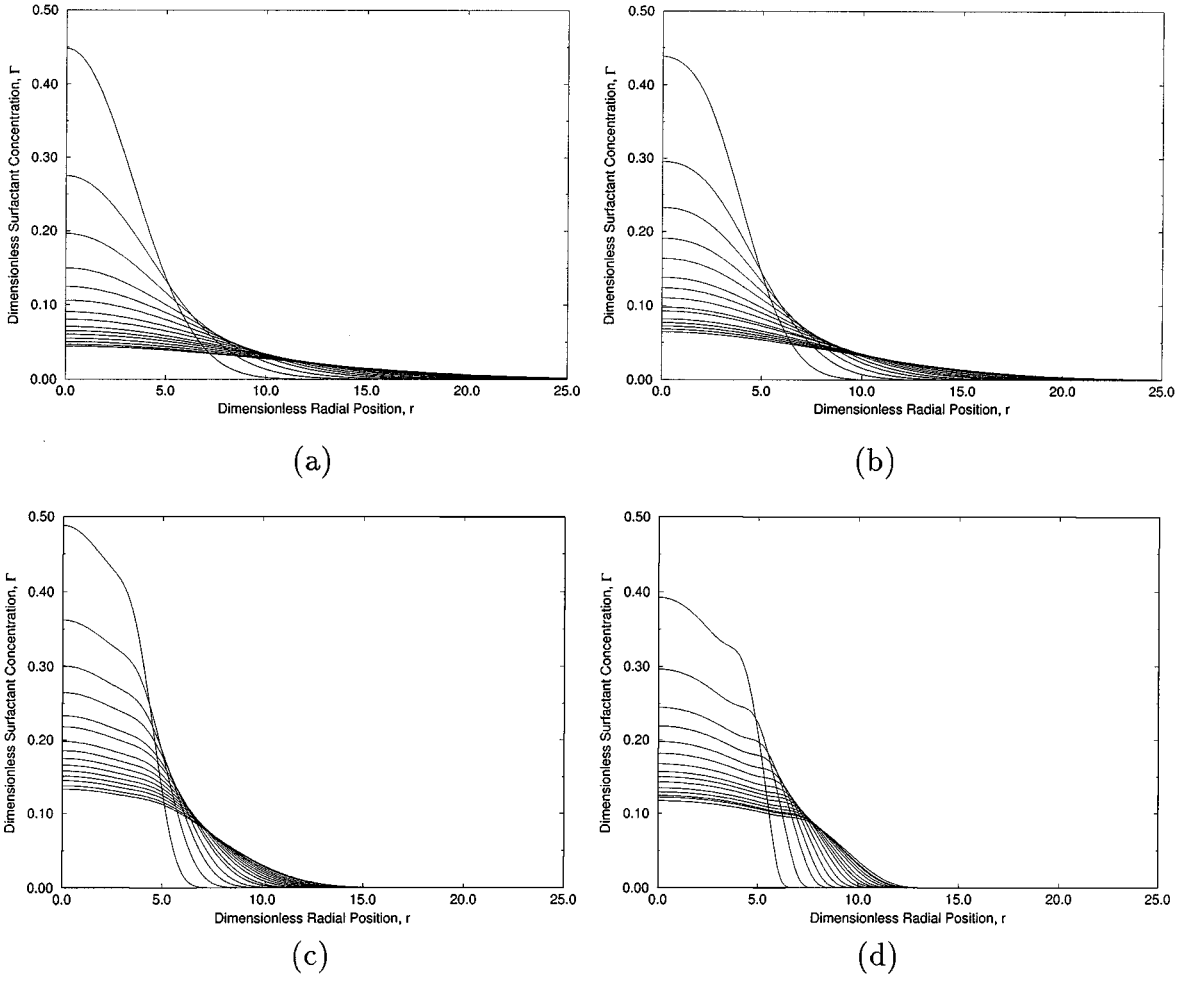

FIG. 11. Surfactant concentration profiles for 15 equal time steps: (a) $\mathrm{Pe}_s = 0.1$, $t = 0$ to 5, (b) $\mathrm{Pe}_s = 1$, $t = 0$ to 30, (c) $\mathrm{Pe}_s = 10$, $t = 0$ to 50, and (d) $\mathrm{Pe}_s = 100$, $t = 0$ to 100. The other parameter values are $\lambda = 1$, $\Gamma_b = 0$, and $B = 0$.

for the case of $B = 1$. Since the disjoining pressure force now plays a dominant factor in film thinning even at early stages subsequent to the initial deformation of the film due to Marangoni forces, the rapid thinning of the film causes liquid to be driven away from both sides of the thinning region. Whereas the outspreading wave due to film thickening at the surfactant leading edge has been observed in previous cases illustrated in Section 3.2.1 where the magnitude of B is moderate, film thickening, in this case, also occurs in the region upstream of the thinning zone. The associated surfactant concentration profile is shown in Fig. 13b. It can be seen that the overall concentration profile does not deviate very significantly from the initial concentration profile because the time scale to rupture is very small due to the large van der Waals attractive force that results in the enhancement of the rate of film thinning. In addition, we observe that the surfactant concentration in the region upstream of the thinning region rises above its initial value, indicating that as the film is driven away from the thinning region toward the center, surfactant is carried with it. Again, it can be seen that at the region of film rupture, there is a sharp depletion of surfactant where Marangoni forces could potentially arise to refill the rupture region and hence prevent film rupture as discussed earlier. However, because the van der Waals force is extremely strong in this case, this does not occur. Instead, the film proceeds to rupture in a very short time span. In the cases we have so far presented as well, these Marangoni forces which act against van der Waals forces are insufficient to stabilize the film against rupture.

We have also studied other cases. Figure 14 represents a typical set of results. It shows the minimum film thickness as a function of the dimensionless Hamaker constant, B, with $\lambda = 1$ and $\mathrm{Pe}_s = 1$ and in the absence of background surfactant concentration. These results indicate that rupture is delayed significantly in the case of weaker van der Waals forces. If van der Waals forces are weak, for example when $B = 1 \times 10^{-3}$, the film does not rupture as the hydrodynamic effects attempting to recover the film curvature replenish the film before the film can thin to a thickness at which the van der Waals force becomes effective. Potential rupture could occur if the dimensionless Hamaker

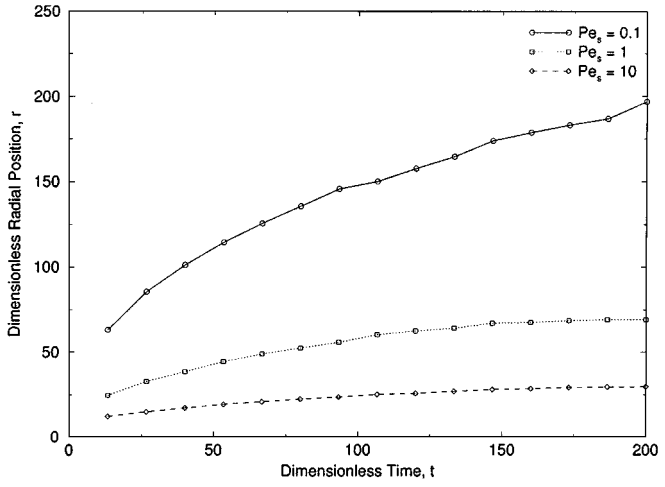

FIG. 12. The effect of varying the surface Péclet number, Pe_s, on the surfactant spreading rate. The other parameter values are $\lambda = 1$, $\Gamma_b = 0$, and $B = 0$.

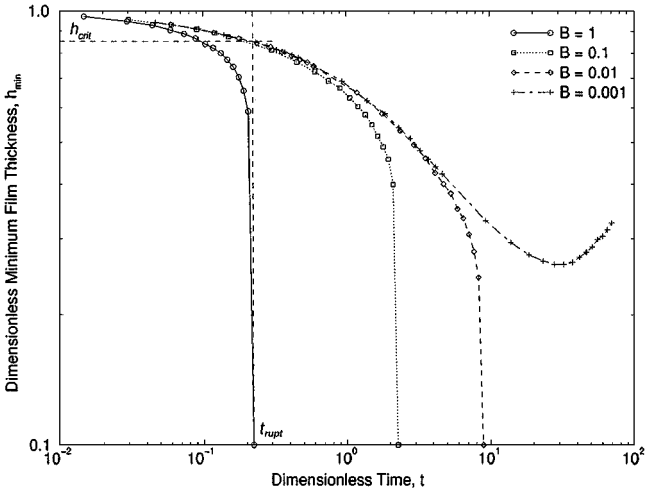

FIG. 14. The effect of varying the dimensionless Hamaker constant, B, on the minimum film thickness. The other parameter values are $\lambda = 1$, $\mathrm{Pe}_s = 1$, and $\Gamma_b = 0$. (The arrows indicate an estimate of the rupture time, t_{rupt}, and the critical film thickness, h_{crit}, for these parameter values.)

constant is in the range $1 \times 10^{-2} < B < 1$ for this set of parameter values. In addition, the rupture time, t_{rupt}, and the critical film thickness, h_{crit}, defined as the values of the minimum film thickness at the rupture time in the absence of van der Waals forces (17), can be estimated as illustrated in Fig. 14. Figure 15 shows the rupture times obtained for various background surfactant concentrations, indicating that the presence of background surfactant slightly delays the film thinning process and hence the onset of rupture. In both figures, we see that the rupture time is of the order 10^{-2} to 1 s. Ruputure times resulting from dimpling films of the order of 1 s to 10 ms have been reported in theoretical work (17) whereas Manev *et al.* (28) have reported experimental coalescence times for aqueous emulsion films of order 100 s. In systems of coalescing bubbles, experimentally determined coalescence times of order 1 to 100 s (13, 29) and 10 to 100 s (28, 30) have been obtained whereas rupture time scales of order 1 s have been found in this study for low viscosity ratios and weak van der Waals forces (see, for example, Fig. 4a where $\lambda = 0.1$ and $B = 1 \times 10^{-2}$).

In general, a comparison between rupture time scales presented in this work with theoretically predicted and experimentally determined rupture time scales for which dimpling is the mechanism for rupture reveals that Marangoni-driven local drainage leading to rupture occurs on slightly faster or, at least, comparable time scales. That is, local variations in the surfactant concentration may result in film rupture, which could give rise to an alternative pathway to drop coalescence.

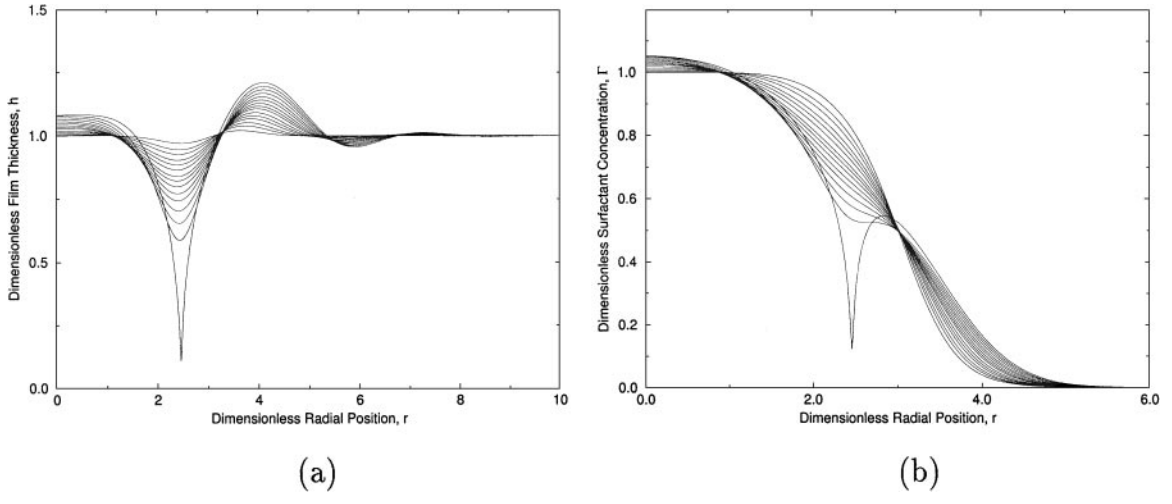

FIG. 13. Film thickness (semi-logarithmic plot) (a) and surfactant concentration (b) profiles for $B = 1$ from $t = 0$ to 0.222 in 15 equal time steps. The other parameter values are $\lambda = 1$, $\mathrm{Pe}_s = 1$, and $\Gamma_b = 0$.

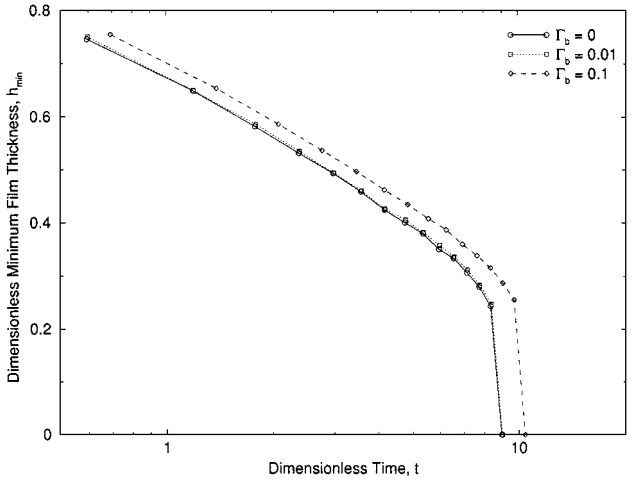

FIG. 15. Rupture times for various background surfactant concentrations, Γ_b. The parameter values are $\lambda = 1$, $\mathrm{Pe}_s = 1$, and $B = 1 \times 10^{-2}$.

4. CONCLUSIONS

In this study, the analysis of Shen and Hartland (18) has been extended to investigate local drainage of a continuous phase liquid film formed between two drops in the presence of interfacial concentration gradients. Contrary to the traditional notion that Marangoni forces generally act to stabilize drops against rupture and coalescence, we have found that the presence of an initially nonuniform distribution of insoluble surfactant at the interface can initiate localized drainage leading to the thinning of the film between the drops.

We have conducted a full parameteric study of the effects of the viscosity ratio, the background surfactant concentration, the surface Péclet number, and the dimensionless Hamaker constant on the drainage process for the case where surfactant is present only in trace amounts. We have found that the influence of surfactant on film drainage is strongest when the dispersed phase viscosity is low compared to that of the continuous phase. This is a consequence of the decreasing retardation effect that the dispersed phase exerts on the spreading of surfactant by Marangoni stresses. The presence of background surfactant at the interface was found to give rise to reverse Marangoni flow, which opposes the outward destabilizing Marangoni flow that results from the imposed surfactant concentration profile, thereby retarding film thinning. Depending on the conditions, this flow reversal was shown to result in refilling of the film.

When the surface Péclet number is small, the effect of surfactant has been found to be negligible as diffusion acts to distribute the surfactant along the interface with little disturbance caused to the film on a time scale much smaller than the time scale at which Marangoni convection takes place. The film therefore recovers subsequently after initial thinning since there are now insufficient stresses arising from interfacial tension gradients to overcome the hydrodynamic effects attempting to recover the drop curvature. For small surface Péclet numbers, the rate of spreading of surfactant is also low compared to the case of large surface Péclet numbers in which Marangoni convection increasingly becomes the dominant mode of surfactant transport; the effect of the Péclet number on the rate of film thinning becomes more and more pronounced as the viscosity ratio is increased. In these cases, we find that there is an enhancement of the interfacial velocity as a result of the interfacial concentration gradient and this leads to rapid thinning of the film.

The possibility of film rupture due to van der Waals forces was also examined. It can be concluded from our results that local film drainage can lead to the rupture of the film and hence drop coalescence if Marangoni stresses can sufficiently thin the film down to thicknesses where van der Waals forces are effective. The time scales for rupture promoted by Marangoni stresses found in this study are shown to be at least comparable to the rupture time scales occurring when dimpling takes place in the approach and collision of two drops, thus suggesting an alternative pathway to drop coalescence via local variations in the surfactant concentration.

APPENDIX: DERIVATION OF THE SIMILARITY SOLUTIONS

It is possible to recast the numerical solutions in terms of similarity variables by first simplifying Eqs. [13] and [18] such that only Marangoni forces are present, that is, in the limits $1/\mathrm{Pe}_s \to 0$ and $\epsilon^2 \gamma_m^*/S^* \to 0$. These equations, along with Eqs. [9] and [21], then reduce to

$$\frac{\partial h}{\partial t} = \frac{1}{r}\frac{\partial}{\partial r}\left[r h \left(\frac{R}{2\lambda}\frac{\partial \Gamma}{\partial r} \right) \right], \qquad [39]$$

$$\frac{\partial \Gamma}{\partial t} = \frac{1}{r}\frac{\partial}{\partial r}\left[r \Gamma \left(\frac{R}{2\lambda}\frac{\partial \Gamma}{\partial r} \right) \right]. \qquad [40]$$

Moreover, the following condition for global conservation of the mass of surfactant, M, is imposed:

$$M = 2\pi \int_0^\infty r \Gamma \, \mathrm{d}r. \qquad [41]$$

We now introduce the following set of similarity scalings (26) into Eqs. [39]–[41]:

$$\xi = \frac{r}{t^a}, \quad h(r,t) = H_0(\xi), \quad \Gamma(r,t) = \frac{G_0(\xi)}{t^b}. \qquad [42]$$

Here, the surfactant leading edge is located at $\xi = 1$. In these transformed coordinates, Eqs. [39]–[41] are rendered time-independent when $2a + b - 1 = 0$ and $2a - b = 0$ for a finite amount of surfactant, M, in axisymmetric geometry. Thus $a = \frac{1}{4}$ and $b = \frac{1}{2}$, implying that the surfactant leading edge advances as $t^{\frac{1}{4}}$, for a finite mass of surfactant.

Equations [39] and [40] can now be written as

$$\left[\frac{1}{\xi}\frac{\partial}{\partial\xi}\left(\frac{\xi H_0 R}{2\lambda}\frac{dG_0}{d\xi}\right)+\frac{\xi}{4}\frac{dH_0}{d\xi}\right]=0, \quad [43]$$

$$\left[\frac{G_0}{2}+\frac{\xi}{4}\frac{dG_0}{d\xi}+\frac{1}{\xi}\frac{d}{d\xi}\left(\frac{\xi R G_0}{2\lambda}\frac{dG_0}{d\xi}\right)\right]=0. \quad [44]$$

Integration of Eq. [44] with the boundary condition $G_0 = 0$ as $\xi \to \infty$ yields

$$\frac{dG_0}{d\xi} = -\frac{\lambda\xi}{2R}\Theta(1-\xi), \quad [45]$$

where $\Theta(1-\xi)$ is the Heaviside function given by

$$\Theta(1-\xi) = \begin{cases} 0 & \text{for } \xi > 1, \\ 1 & \text{otherwise.} \end{cases} \quad [46]$$

Equation [45] implies that $dG_0/d\xi = -\lambda/2R$ for $\xi \le 1$ and $dG_0/d\xi = 0$ for $\xi > 1$. The following boundary condition also applies: $H_0 = 1$ and $G_0 = 0$ for $\xi > 1$. Substituting Eq. [45] into Eq. [43] yields the expression

$$\xi^2\frac{dH_0}{d\xi} - \frac{d}{d\xi}[\xi^2 H_0\Theta(1-\xi)] = 0. \quad [47]$$

By seeking a solution of the form

$$H_0 = \Theta(1-\xi)f(\xi) - g(\xi) + 1, \quad [48]$$

it can be shown that

$$\Theta(1-\xi)f(\xi) = \frac{\delta(1-\xi)}{2} \quad [49]$$

and

$$g(\xi) = \Theta(1-\xi), \quad [50]$$

where $\delta(1-\xi)$ is the Dirac delta function given by

$$\delta(1-\xi) = \begin{cases} \infty & \text{at } \xi = 1, \\ 0 & \text{otherwise.} \end{cases} \quad [51]$$

The similarity solution for the evolution of the film thickness is therefore

$$H_0 = \frac{\delta(1-\xi)}{2} - \Theta(1-\xi) + 1. \quad [52]$$

Since the position of the shock has been assumed to occur at $\xi = 1$ and is determined by the total surfactant mass, we can normalize the similarity scalings given in Eq. [42] using the transformation (26)

$$h(r,t) = H(\xi,\tau), \quad \xi = \frac{r}{\xi_s t^a},$$
$$\Gamma(r,t) = \frac{\xi_s^2 G(\xi,\tau)}{t^b}, \quad t = \tau, \quad [53]$$

such that the position of the shock in the original coordinate system, x_s, is given by

$$x_s = \xi_s(Q)t^a, \quad [54]$$

where Q is defined by

$$Q = \frac{M}{t^c}, \quad [55]$$

where $c = 0$ for a finite amount of surfactant. It then follows from Eq. [41] that, for $c = 0$,

$$\xi_s = \left(\frac{Q}{2\pi\int_0^\infty \xi G\, d\xi}\right)^{\frac{1}{4}}, \quad [56]$$

which, upon normalization, gives

$$\xi_s = \left(\frac{Q}{2\pi\int_0^1 \xi G_0\, d\xi}\right)^{\frac{1}{4}}. \quad [57]$$

Integration of Eq. [45] then yields

$$\xi_s = \left(\frac{4RQ}{\lambda\pi}\right)^{\frac{1}{4}}. \quad [58]$$

REFERENCES

1. Kitchener, J. A., *in* "Recent Progress in Surface Science" (J. F. Danielli, K. G. A. Pankhurst, and A. C. Riddiford, Eds.), Vol. 1, p. 51. Academic Press, London, 1964.
2. Sheludko, A., *Adv. Colloid Interface Sci.* **1,** 391 (1967).
3. Clunie, J. S., Goodman, J. F., and Ingram, B. T., *in* "Surface and Colloid Science" (E. Matijević, Ed.), Vol. 3, p. 167. Wiley, New York, 1971.
4. Ivanov, I. B., and Jain, R. K., *in* "Dynamics and Instability of Fluid Interfaces" (T. S. Sørensen, Ed.), p. 120. Springer-Verlag, Berlin, 1979.
5. Jain, R. K., Ivanov, I. B., Maldarelli, C., and Ruckenstein, E., *in* "Dynamics and Instability of Fluid Interfaces" (T. S. Sørensen, Ed.), p. 140. Springer-Verlag, Berlin, 1979.
6. Wasan, D. T., and Malhotra, A. K., *AIChE Symp. Seri.* **82**(252), 5 (1986).
7. Chen, J. D., *J. Colloid Interface Sci.* **107**(1), 209 (1985).
8. Li, D., *J. Colloid Interface Sci.* **163,** 108 (1994).
9. Klaseboer, E., Chevaillier, J. Ph., Gourdon, C., and Masbernat, O., *J. Colloid Interface Sci.* **299,** 274 (2000).
10. Radoëv, B. P., Dimitrov, D. S., and Ivanov, I. B., *Colloid Polym. Sci.* **252,** 50 (1974).
11. Traykov, T. T., and Ivanov, I. B., *Int. J. Multiphase Flow* **3,** 471 (1977).
12. Sharma, A., and Ruckenstein, E., *Colloid Polym. Sci.* **266,** 60 (1988).
13. Li, D., *J. Colloid Interface Sci.* **181,** 34 (1996).

14. Danov, K. D., Valkovska, D. S., and Ivanov, I. B., *J. Colloid Interface Sci.* **211,** 291 (1999).
15. Valkovska, D. S., Danov, K. D., and Ivanov, I. B., *Colloid Surf. A* **175,** 179 (2000).
16. Ivanov, I. B., Dimitrov, D. S., Somasundaran, P., and Jain, R. K., *Chem. Eng. Sci.* **40**(1), 137 (1985).
17. Chesters, A. K., and Bazhlekov, I. B., *J. Colloid Interface Sci.* **230,** 229 (2000).
18. Shen, H., and Hartland, S., *J. Colloid Interface Sci.* **167,** 94 (1994).
19. Li, D., and Liu, S., *Langmuir* **12,** 5216 (1996).
20. Jeelani, S. A. K., and Hartland, S., *J. Colloid Interface Sci.* **206,** 83 (1998).
21. Milliken, W. J., Stone, H. A., and Leal, L. G., *Phys. Fluids A* **5**(1), 69 (1993).
22. Chen, J. D., and Slattery, J. C., *AIChE J.* **28**(6), 955 (1982).
23. Lin, C. Y., and Slattery, J. C., *AIChE J.* **28**(1), 147 (1982).
24. Schiesser, W. E., "The Numerical Method of Lines." Academic Press, San Diego, 1991.
25. Matar, O. K., and Troian, S. M., *Phys. Fluids A* **11,** 3232 (1999).
26. Jensen, O. E., and Grotberg, J. B., *J. Fluid Mech.* **240,** 259 (1992).
27. Gaver, D. P., and Grotberg, J. B., *J. Fluid Mech.* **213,** 127 (1990).
28. Manev, E. D., Sazdanova, S. V., and Wasan, D. T., *J. Colloid Interface Sci.* **97**(2), 591 (1984).
29. Li, D., *Chem. Eng. Sci.* **51**(14), 3623 (1996).
30. Li, D., and Slattery, J. C., *AIChE J.* **34**(5), 862 (1988).